Smart Structures and Systems, *Vol. 26, No. 2 (2020) 195-211*
DOI: https://doi.org/10.12989/sss.2020.26.2.195

Vertical equipment isolation using piezoelectric inertial-type isolation system

Lyan-Ywan Lu*[1], Ging-Long Lin[2a], Yi-Siang Chen[3b] and Kun-An Hsiao[1c]

[1] *Department of Civil Engineering, National Cheng Kung University, 1 University Road, Tainan 701, Taiwan*
[2] *Department of Construction Engineering, National Kaohsiung University of Science and Technology, 1 University Road, Kaohsiung 824, Taiwan*
[3] *Department of Civil and Construction Engineering, National Taiwan University of Science and Technology, 43 Keelung Road, Sec. 4, Taipei 106, Taiwan*

(*Received November 6, 2019, Revised March 14, 2020, Accepted May 27, 2020*)

Abstract. Among anti-seismic technologies, base isolation is a very effective means of mitigating damage to structural and non-structural components, such as equipment. However, most seismic isolation systems are designed for mitigating only horizontal seismic responses because the realization of a vertical isolation system (VIS) is difficult. The difficulty is primarily due to conflicting isolation stiffness demands in the static and dynamic states for a VIS, which requires sufficient rigidity to support the self-weight of the isolated object in the static state, but sufficient flexibility to lengthen the isolation period and uncouple the ground motion in the dynamic state. To overcome this problem, a semi-active VIS, called the piezoelectric inertia-type vertical isolation system (PIVIS), is proposed in this study. PIVIS is composed of a piezoelectric friction damper (PFD) and a leverage mechanism with a counterweight. The counterweight provides an uplifting force in the static state and an extra inertial force in the dynamic state; therefore, the effective vertical stiffness of PIVIS is higher in the static state and lower in the dynamic state. The PFD provides a controllable friction force for PIVIS to further prevent its excessive displacement. For experimental verification, a shaking table test was conducted on a prototype PIVIS controlled by a simple controller. The experimental results well agree with the theoretical results. To further investigate the isolation performance of PIVIS, the seismic responses of PIVIS were simulated numerically by considering 14 vertical ground motions with different characteristics. The responses of PIVIS were compared with those of a traditional VIS and a passive system (PIVIS without control). The numerical results demonstrate that compared with the traditional and passive systems, PIVIS can effectively suppress isolation displacement in all kinds of earthquake with various peak ground accelerations and frequency content while maintaining its isolation efficiency. The proposed system is particularly effective for near-fault earthquakes with long-period components, for which it prevents resonant-like motion.

Keywords: vertical isolation; leverage mechanism; piezoelectric actuator; semi-active friction damper; inertia type; near-fault earthquake; anti-resonance

1. Introduction

For critical facilities, such as medical institutions, power plants, and industrial facilities, the seismic performance of non-structural components, such as equipment and pipelines, is as important as that of the structure itself, since for maintaining the functionality of these facilities, the non-structural components have to be undamaged after the earthquake. Studies have shown that vertical ground motions, which usually exhibit more high-frequency components than those of horizontal ground motions, are more likely to cause severe damage to non-structural components (Papazoglou and Elnashai 1996, Badalouka and Papadopoulos 2008, FEMA 2011), such as equipment (Memari *et al*. 2004, Furukawa *et al*. 2013), because most non-structural components are high-frequency components.

Furthermore, the vertical component of earthquakes may cause a large amount of slippage or overturning of equipment, which are the primary failure modes for freestanding equipment (Taniguchi and Miwa 2004, Konstantinidis and Makris 2009). Equipment damage due to slippage or overturning may be worsened by floor acceleration amplified by the dynamic effect of the underlying primary structure (Franke *et al*. 2005, Sankaranarayanan and Medina 2007). Although anchoring equipment to the floor may avoid slippage or overturning under seismic excitation, it may lead to large equipment acceleration and high-frequency responses, particularly when the dynamic amplification effect of the underlying structure is considered (Konstantinidis and Makris 2005).

Seismic isolation may be an effective means of protecting equipment. Seismic isolation reduces the seismic load on the isolated object by introducing a soft isolation layer that lengthens the vibration period of the isolated object and thus reduces its response. Nevertheless, most existing seismic isolation systems are designed for horizontal isolation. Studies and applications of vertical isolation systems (VISs) are relatively few due to the conflicting demands of vertical stiffness for such systems. A

*Corresponding author, Professor,
E-mail: lylu@ncku.edu.tw
[a] Assistant Professor
[b] Master of Science
[c] Master of Science

http://www.techno-press.org/?journal=sss&subpage=7
ISSN: 1738-1584 (Print), 1738-1991 (Online)

VIS must have sufficient vertical rigidity to support the self-weight of the isolated object, but must also have sufficient vertical flexibility to lengthen the vibration period under vertical seismic excitation.

Several studies have developed VISs. Kitamura *et al.* (2005) proposed a VIS composed of large coned-disk springs that provide high stiffness at small deformation and low stiffness at large deformation; therefore, sufficient stiffness in the static state and sufficient flexibility in the dynamic state can be achieved. Fujita (1996) proposed a three-dimensional (3D) seismic isolation system that consisted of rubber bearings for the horizontal direction and coned-disc springs for the vertical direction. The experimental results showed that the isolation system is effective in reducing both vertical and horizontal acceleration responses. However, in the above studies, the isolation displacement provided by nonlinear coned-disc springs is usually quite limited. Shimada *et al.* (2004) proposed a 3D isolation system for nuclear reactor buildings. For the vertical direction of this system, the weight of the isolated structure is supported by a load-carrying hydraulic cylinder connected to a gas accumulator via a rocking-suppression cylinder. Vertical isolation thus functions on the principle of an air cushion, and meanwhile horizontal isolation is provided by laminated rubber bearings. Xu *et al.* (2011) proposed a multi-dimensional isolation device that can vertically isolate long-span reticulated structures. The device consists of vertical viscoelastic dampers and a viscoelastic core bearing that has higher energy dissipation ability than that of a traditional rubber bearing. The device allows 8 mm of movement perpendicular to the vertical dampers. Wang *et al.* (2015) applied laminated rubber bearings with thick rubber layers to reduce the vertical frequency of the isolated object. Because the allowable vertical deformation of the rubber bearings is relatively small, the vertical isolator stroke may be limited. Tsuji *et al.* (2014) proposed a nonlinear VIS with a post-buckled beam. The isolator is sufficiently stiff statically to support the self-weight of the isolated object and is soft dynamically to provide a low natural frequency. The isolation performance of the system was investigated using a finite element model with harmonic excitations. For the seismic protection of equipment, Lu *et al.* (2016) proposed a VIS with a leverage mechanism and a counterweight to reduce the initial settlement due to the self-weight of isolated object.

Araki *et al.* (2011) developed a vertical-horizontal base isolation system, in which the vertical isolator is made of vertical constant-force springs and a link mechanism to prevent rocking motion. Constant-force springs are employed to reduce the settlement caused by the static self-weight of the isolated object. Araki *et al.* (2013) later proposed a vertical quasi-zero stiffness (QZS) isolation system that consists of constant-force springs and a pair of hexagonal plates by which the force of the horizontally placed springs can be converted into the vertical restoring force of the isolator. With the high initial stiffness in QZS, excessive static deformation of the isolator is avoided. If the weight of the isolated object changes, the vertical restoring force can be adjusted using cranks and a screw jack. Asai *et al*. (2017) also proposed a QZS isolation system that consists of horizontally placed constant-force springs and a variable ellipse curve mechanism, which can convert the horizontal spring force to the vertical restoring force of the vibration isolator. In addition, the vertical restoring force can be adjusted by changing the ratio of the semi-minor axis to the semi-major one of the ellipse. Zhou *et al*. (2016) examined several vertical and 3D isolation systems and their potential application to modern nuclear facilities. They found that compared with general horizontal isolators, a vertical isolator with a vertical frequency of less than 3 Hz can more effectively reduce the vertical in-structure responses for the studied nuclear facilities. If the vertical frequency of isolators is reduced to 1 Hz, the rocking effect is obvious and rocking restraining devices are necessary.

Moreover, the development of vertical isolation technology also faces a challenge for near-fault ground motions. Recent studies have revealed that near-fault ground motions, which usually contain a strong long-period pulse waveform, may induce a resonance-like response in a long-period horizontal isolation system (Lu *et al*. 2013a). This resonance-like response causes excessive isolator displacement for a horizontal isolation system far beyond the design level, and thus increases the failure risk of the isolation system itself (Jangid and Kelly 2001). A VIS may face a similar problem because vertical near-fault ground motions may have characteristics similar to those of horizontal near-fault earthquakes (Li *et al*. 2007). To overcome this near-fault problem for isolation systems, many improved isolation strategies have been proposed for horizontal isolation systems, including the addition of supplemental damping to mitigate the possible resonant response (Makris and Chang 2000, Lu *et al*. 2013a); the use of a passive variable isolation system, such as variable-stiffness sliding isolators, to avoid resonant behavior (Murnal and Sinha 2004, Soni *et al*, 2011, Lu *et al*. 2011a, 2013b); the use of an active isolation system that can provide an active control force in the isolation layer, so that the isolation performance can be ensured even for near-fault earthquakes (Riley *et al*. 1998, Chang *et al*. 2014); the use of a semi-active isolation system, which is usually formed by incorporating a semi-active device, such as variable damping or variable stiffness device, into the isolation system (Narasimhan and Nagarajaiah 2005, Narasimhan *et al*. 2006, Lu *et al*. 2011b, 2012, Lin *et al*. 2015, 2018). Compared with an active system, a semi-active isolation system can also be adaptive to external excitations with less control energy and greater control stability. Although the above isolation strategies have been proven to be effective for mitigating near-fault isolation responses, they have not been applied to a VIS.

In order to further improve the performance of vertical isolation systems under near-fault earthquakes, the current study is a continuous work of the article by Lu *et al*. (2016), in which a passive inertial-type VIS was investigated, while in the current study, a semi-active VIS using piezoelectric material was proposed and studied experimentally for the seismic protection of equipment. The proposed semi-active VIS, which is called the piezoelectric inertia-type vertical isolation system (PIVIS) is composed of a piezoelectric friction damper (PFD), a leverage mechanism, and a counterweight. The counterweight and leverage mechanism provide an uplifting force in the static state and an extra inertial force in the dynamic state; therefore, the effective vertical stiffness of the system is higher in the static state and lower in the dynamic state. The PFD provides a controllable friction damping force to mitigate excessive isolator displacement of PIVIS, which may be induced by long-period ground motions, such as near-fault earthquakes. A piezoelectric material is used as the control device because it is lightweight, responsive, low-cost, and easy to implement. Piezoelectric materials are widely applied in the active/semi-active control of structural vibrations and smart structural systems (Song *et al*. 2006, Lu *et al*. 2011c, Ramadan *et al*. 2014, Chu *et al*. 2018).

The rest of this paper is organized as follows. The configuration and mathematical model of PIVIS are introduced in Section 2, and the equation of motion is derived in Section 3. The numerical analysis method and the control law for PIVIS are discussed in Sections 4 and 5, receptively. Experimental verification using a shaking table test conducted on a prototype PIVIS is described in Section 6. Using the developed numerical method, Section 7 investigates the isolation performance of PIVIS by comparing it with those of a traditional VIS and a passive PIVIS. Finally, conclusions are presented in Section 8.

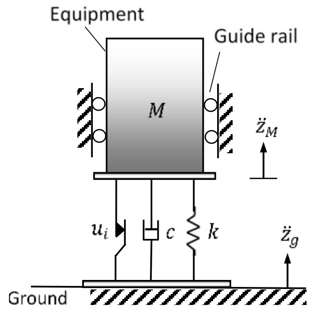

Fig. 1 Mathematical model of a traditional vertical isolation system

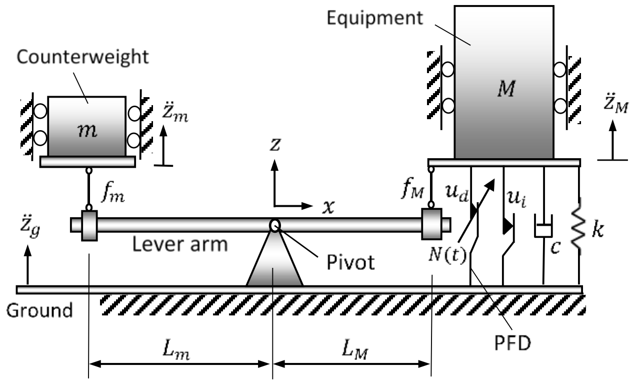

Fig. 2 Mathematical model of PIVIS

2. Piezoelectric inertia-type vertical isolation system

2.1 Configuration and mathematical model of PIVIS

The configuration of PIVIS is described in this section. To highlight the characteristics of PIVIS, Fig. 1 shows the mathematical model of a traditional VIS, which is usually composed of a stiffness element with spring constant k, a viscous damping element with damping coefficient c, a friction element with friction force u_i, and isolated equipment of mass M. The stiffness element provides a vertical restoring force and a soft layer to mitigate the upward transmission of vertical ground acceleration to the isolated equipment. In practice, the stiffness element must be sufficiently soft in the dynamic state but sufficiently stiff in the static state to avoid excessive vertical settlement due to the self-weight of the isolated equipment. The friction element is used to simulate the inherent friction of the guide rails. The damping and friction elements in Fig. 1 provide the required energy dissipation ability to reduce isolation displacement under earthquakes.

Fig. 2 shows the mathematical model of PIVIS. PIVIS is composed of a counterweight of mass m, a leverage mechanism of length (L_m + L_M), and a PFD with friction force u_d, in addition to the components shown in Fig. 1. The clamping force $N(t)$ of the PFD is controllable. In static state, the counterweight and leverage mechanism create an uplifting force, which prevents excessive initial settlement due to the self-weight of the equipment. When PIVIS is excited by a ground motion, the inertial force exerted by the motion of the counterweight and transmitted through the leverage mechanism lengthens the isolation period of PIVIS. Furthermore, using an embedded piezoelectric actuator, the PFD provides a controllable friction force in real time, allowing the vibration energy of PIVIS to be more efficiently dissipated and the dynamic isolator displacement to be further reduced without affecting isolation efficiency. In summary, PIVIS can prevent excessive isolation displacement in both static and dynamic states and provide an adaptive damping force through the PFD under extreme earthquake events.

2.2 Prototype of PIVIS

Fig. 3 shows the prototype of PIVIS used in the test. The prototype mainly consists of a leverage platform system, a suspended isolation spring, and a PFD. These components are described below:

(1) Leverage platform system: As shown in Fig. 3, this system includes a leverage mechanism that has a vertical guide rod and a platform at each of its two ends. The leverage mechanism contains a rigid lever arm and a pivot hinge fixed to a supporting base that is mounted on the ground or a building floor. The platforms at the two ends of the lever arm are used for the installation of equipment and the counterweight, respectively. The vertical guide rods restrict the motion of the equipment and the counterweight in the vertical direction. The rigid lever arm transmits the inertial force of the counterweight to the isolated equipment, providing a passive reactive force to suppress equipment motion.

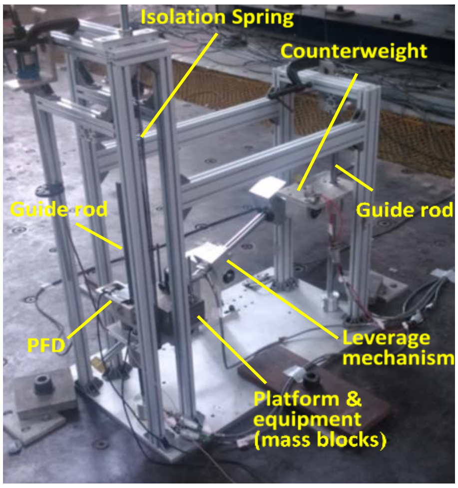

Fig. 3 Photo of prototype PIVIS

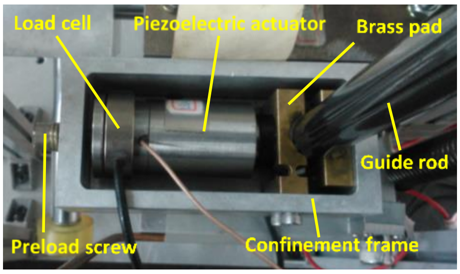

Fig. 4 Interior of piezoelectric friction damper (PFD)

(2) Suspended isolation spring: The isolation spring suspended from the top of the frame is connected to the equipment platform to support the equipment self-weight in the static state and to provide a restoring force during an earthquake.

(3) Piezoelectric friction damper: As shown in Fig. 4, the PFD is composed of a piezoelectric actuator, a pair of brass pads (clip), a pre-load screw, and a load cell. The pair of brass clips together with the guide rod provide a stable friction damping force. The piezoelectric actuator, which is driven by a voltage amplifier, creates a controllable clip force on the friction pads and the pre-load screw provides an initial clip force. The load cell is employed to measure the total clip force of the PFD.

3. Theory of PIVIS

3.1 Derivation of dynamic equation

To analyze seismic behavior and assess the isolation performance of PIVIS, the equation of motion of PIVIS is derived in this section. In Fig. 2, if we consider the free body diagrams of the counterweight m and equipment M, respectively, the dynamic equilibrium equation for these two mass blocks can be written as

$$\sum F_z = f_m(t) - mg = m(\ddot{z}_g(t) + \ddot{z}_m(t)) \tag{1}$$

$$\begin{aligned}\sum F_z = f_M(t) - c\,\dot{z}_M(t) - k\,z_M(t) - u_i(t) \\ -u_d(t) - Mg = M\,(\ddot{z}_g(t) + \ddot{z}_M(t))\end{aligned} \tag{2}$$

where f_m and f_M represent the reaction forces applied to the counterweight and equipment through the lever arm, respectively; $\ddot{z}_g$ is the vertical ground acceleration; z_m and z_M denote the vertical displacements of the counterweight and equipment with respect to the ground, respectively; g is gravitational acceleration; k is the stiffness of the isolation spring; u_i denotes the inherent friction force due to the sliding of guide rails and rotation of the pivot; and u_d represents the friction force provided by the PFD. Of note, the sign convention for quantities f_m, f_M, z_m, and z_M is defined as positive upward.

Furthermore, considering the free body diagram of the lever arm alone, as shown in Fig. 5, and ignoring the mass of the lever arm, from the moment-balance condition we have

$$f_M(t) = R_L f_m(t) \tag{3}$$

where R_L is the moment-arm ratio, defined as

$$R_L = \frac{L_m}{L_M} \tag{4}$$

Additionally, from the geometric configuration in Fig. 5, we have

$$z_m(t) = -R_L z_M(t) \tag{5}$$

Finally, substituting Eqs. (1), (2), and (5) into Eq. (3) yields the following overall dynamic equation for the entire PIVIS

$$\begin{aligned}(1 + RR_L)M\ddot{z}_M(t) + c\dot{z}_M(t) + kz_M(t) + (1 - R)Mg \\ = -(1 - R)M\ddot{z}_g(t) - u_i(t) - u_d(t)\end{aligned} \tag{6}$$

where

$$R = \frac{mL_m}{ML_M} \tag{7}$$

In the above equations, R denotes the ratio of the static moments acting on the two sides of the lever arm. Of note, Eq. (6) is a single-degree-of-freedom equation. If the counterweight and PFD are removed, i.e., $R = 0$ (or $m = 0$) and $u_d = 0$, Eq. (6) reduces to the dynamic equation of the traditional VIS shown in Fig. 1. Equation (6) states that the dynamic equation of PIVIS can be attenuated by changing parameters R and R_L.

3.2 Static property of PIVIS

Because a seismic isolation system is at rest most of the time, understanding the static behavior of PIVIS is important. To this end, substituting $\ddot{z}_M = \dot{z}_M = \ddot{z}_g = 0$ into Eq. (6) and ignoring the friction effect, i.e., $u_i = u_d = 0$, for the time being, Eq. (6) is reduced to the following static equilibrium equation for PIVIS

$$z_{M,0} = \frac{-Mg}{k_s} \tag{8}$$

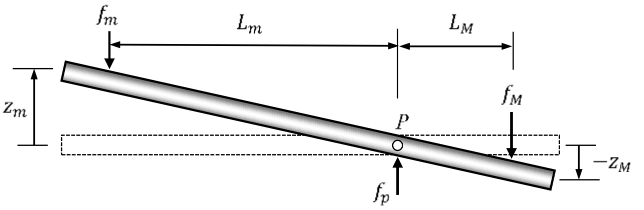

Fig. 5 Free body diagram of lever arm

where $z_{M,0}$ represents the initial settlement of PIVIS in the static state, and k_s denotes the equivalent static stiffness, defined as

$$k_s = \frac{k}{(1-R)} > k \quad (\text{for } 0 < \mathrm{R} < 1) \tag{9}$$

Eqs. (8) and (9) indicate that when the value of R increases from 0 to 1, the equivalent static stiffness k_s increases and the static settlement $z_{M,0}$ decreases. Therefore, a higher equivalent static stiffness and a smaller initial settlement can be achieved by adjusting R to reduce the total stroke demand on the isolation spring. Because R = 0 represents a traditional VIS, PIVIS always has a lower $z_{M,0}$ demand than that of a traditional VIS.

3.3 Dynamic property of PIVIS

To investigate the dynamic characteristics of PIVIS more clearly, let us remove the static settlement (neutral position) $z_{M,0}$ from the system response by rewriting the response $z_M(t)$ as

$$z_M(t) = \Delta z_M(t) + z_{M,0} \tag{10}$$

where $\Delta z_M(t)$ denotes the dynamic displacement of PIVIS around the neutral position $z_{M,0}$. Substituting Eqs. (10), (8), and (9) into Eq. (6), and after the substitution replacing $\Delta z_M(t)$ by $z_M(t)$ to simplify the notation, Eq. (6) can be rewritten as the following dimensionless equation

$$\begin{aligned} &\ddot{z}_M(t) + 2\bar{\zeta}\bar{\omega}\dot{z}_M(t) + \bar{\omega}^2 z_M(t) \\ &= -\alpha\ddot{z}_g(t) - \frac{1}{(1+RR_L)M}(u_i(t) + u_d(t)) \end{aligned} \tag{11}$$

where

$$\begin{aligned} &\bar{\omega} = \sqrt{\frac{\bar{k}}{M}} = \frac{\omega}{\sqrt{1+RR_L}}, \quad \bar{k} = \frac{k}{(1+RR_L)}, \quad \omega = \sqrt{\frac{k}{M}}, \\ &\alpha = \frac{1-R}{1+RR_L}, \quad \bar{\zeta} = \frac{\zeta}{\sqrt{1+RR_L}}, \quad \zeta = \frac{c}{2M\omega} \end{aligned} \tag{12}$$

In Eq. (11), $z_M(t)$ is the dynamic displacement of PIVIS after the static settlement is removed; α represents the influence factor of the ground excitation; $\bar{k}$ is the equivalent dynamic stiffness of PIVIS; $\bar{\omega}$ and $\bar{\zeta}$ are the equivalent isolation frequency and equivalent damping ratio of PIVIS, respectively; and ω and ζ are the original isolation frequency and damping ratio without the counterweight, respectively. Of note, ω and ζ also represent the frequency and damping of a counterpart traditional VIS.

From Eq. (12), the equivalent dynamic stiffness $\bar{k}$ is affected by parameters R and R_L, and from Eqs. (4) and (7), the values of R_L and R cannot be negative (i.e.,$R_L \geq 0$ and $R \geq 0$); therefore, we have

$$\bar{k} \leq k \tag{13}$$

The above equation states that the dynamic stiffness k of PIVIS is always less than or equal to the original stiffness k due to the existence of the counterweight. In other words, in the dynamic state, PIVIS is a softer system that has a longer isolation period than that of its traditional counterpart. A longer isolation period usually leads to better isolation performance. In summary, Eqs. (9) and (13) together state that by selecting suitable parameters R and R_L, PIVIS achieves higher equivalent stiffness in the static state to reduce the initial settlement and lower equivalent stiffness in the dynamic state to retain better isolation efficiency.

Moreover, in Eq. (11), the ground acceleration is multiplied by the factor α, which can be treated as an influence factor of seismic force. Because R is usually taken to be 0 < R < 1, from the definition of α in Eq. (12), we have

$$\alpha < 1 \qquad (\text{for} \quad 0 \leq R < 1) \tag{14}$$

Eq. (14) indicates that the ground excitation is reduced by the factor α, which is a function of parameters R and R_L.

Based on the above discussion, it can be concluded that R and R_L are the two important design parameters of PIVIS because both the static and dynamic properties of the system relies on them. From Eq. (11), the dynamic response of PIVIS can also be attenuated by the controllable friction force u_d, which is a semi-active control force provided by the PFD. The magnitude of u_d is determined in real time by a control law. The control law employed in the experiment is described in a later section.

4. Numerical analysis method

4.1 Discrete-time state-space equation

The dynamic equation of PIVIS shown in Eq. (11) is actually nonlinear due to the existence of the friction force $u_i(t) + u_d(t)$. A numerical simulation method that can deal with this nonlinearity is described in this section. First, the second-order dynamic equation Eq. (11) is rewritten in a first-order state-space form

$$\dot{\boldsymbol{z}}(t) = \boldsymbol{A}\boldsymbol{z}(t) + \boldsymbol{B}u(t) + \boldsymbol{E}\ddot{z}_g(t) \tag{15}$$

where $\dot{\boldsymbol{z}}(t)$ is the state vector; A denotes the system matrix; and **B** and **E** represent the influence vectors associated with friction force and seismic excitation, respectively. These matrices are

$$\begin{aligned} &\boldsymbol{z}(t) = \begin{bmatrix} \dot{z}_M \\ z_M \end{bmatrix}, \qquad \boldsymbol{A} = \begin{bmatrix} -2\bar{\zeta}\bar{\omega} & -\bar{\omega}^2 \\ 1 & 0 \end{bmatrix}, \\ &\boldsymbol{B} = \begin{bmatrix} \dfrac{-1}{(1+RR_L)M} \\ 0 \end{bmatrix}, \quad \boldsymbol{E} = \begin{bmatrix} -\alpha \\ 0 \end{bmatrix} \end{aligned} \tag{16}$$

and $u(t)$ denotes the total friction force, i.e.

$$u(t) = u_i(t) + u_d(t) \tag{17}$$

Eq. (15) is the state-space equation of PIVIS, which is a semi-active system. However, if the semi-active damping force is set to zero, i.e., $u_d(t) = 0$, Eq. (15) represents a passive PIVIS. If both $u_d(t)$ and R are set to zero, i.e., $u_d(t) = R = 0$, Eq. (15) reduces to a traditional VIS. Moreover, for convenience of numerical simulation, the discrete-time solution for Eq. (15) is given in the following incremental form

$$\boldsymbol{z}[k+1] = \boldsymbol{A}_d \boldsymbol{z}[k] + \boldsymbol{B}_d u[k] + \boldsymbol{E}_d \ddot{z}_g[k] \tag{18}$$

where $\cdot[k]$ denotes that the associated quantity is evaluated at the k-th time step, and symbols $\boldsymbol{A}_d$, $\boldsymbol{B}_d$, and $\boldsymbol{E}_d$ represent the discrete-time matrices associated with matrices **A**, **B**, and **E**, respectively, i.e.

$$\begin{aligned} &\boldsymbol{A}_d = e^{A\Delta t}, \quad \boldsymbol{B}_d = \boldsymbol{A}^{-1}(\boldsymbol{A}_d - \boldsymbol{I})\boldsymbol{B}, \\ &\boldsymbol{E}_d = \boldsymbol{A}^{-1}(\boldsymbol{A}_d - \boldsymbol{I})\boldsymbol{E} \end{aligned} \tag{19}$$

4.2 Computation of friction force u[k]

In Eq. (18), the state vector at the next time step $\boldsymbol{z}[k+1]$ is determined by the state $\boldsymbol{z}[k]$, friction force $u[k]$, and ground acceleration $\ddot{z}_g[k]$ at the previous step. However, friction force $u[k]$ is an unknown at the beginning of the computation of the (k+1)-step. In this section, the numerical approach used to determine $u[k]$ at each time step is described.

From the mathematical model shown in Fig. 2, it is known that due to the existence of friction forces, and thus the motion of PIVIS includes a sliding state and a sticking (non-sliding) state. According to Coulomb's friction law, PIVIS will remain in its sticking state if at any time instant the total friction force $u[k]$ is less than the maximum sticking force of the friction interface; otherwise, PIVIS will enter its sliding state and the friction force will be equal to the sliding force. Because the PIVIS friction force $u[k]$ includes $u_d[k]$ (PFD friction force) and $u_i[k]$ (inherent friction) (see Eq. (17)), the magnitude of the total friction $u[k]$ should be less than its maximum value $u_{max}[k]$ (sliding force)

$$|u[k]| \le u_{\max}[k] = u_{i,\max} + u_{d,\max}[k] \tag{20}$$

where $u_{i,max}$ and $u_{d,max}$ represent the maximum values of the inherent friction u_i and the PFD friction u_d, respectively. $u_{i,max}$ is a constant, whereas $u_{d,max}$ is a time-varying quantity that can be controlled by the piezoelectric actuator embedded in the PFD. The magnitude of $u_{d,max}$, which is also called the slip force of the PFD, is determined by a given control law, which is discussed in the next section.

In Eq. (18), to determine the total friction force $u[k]$ of PIVIS at each time step, the shear force balance method (Lu *et al.* 2006), which is a very efficient numerical method for dealing with a dynamic system with friction elements, is employed. In this method, it is assumed that from the k-th to (k+1)-th time step PIVIS is in its sticking state, and thus the sliding velocity of the isolated equipment relative to the ground must be equal to zero, i.e.

$$\dot{z}_M[k+1] = \boldsymbol{D}_1\, \boldsymbol{z}[k+1] = 0 \tag{21}$$

where $\boldsymbol{D}_1 = [1 \;\; 0]$. By substituting Eq. (18) into Eq. (21), the friction force $\tilde{u}[k]$ under the assumption of the sticking state can be solved as

$$\tilde{u}[k] = -(\boldsymbol{D}_1\boldsymbol{B}_d)^{-1}\boldsymbol{D}_1(\boldsymbol{A}_d\boldsymbol{z}[k] + \boldsymbol{E}_d\ddot{z}_g[k]) \tag{22}$$

According to Coulomb's friction law, the magnitude of the friction force on a friction interface cannot exceed its maximum sticking force (sliding force); therefore, if $|\tilde{u}[k]| \le u_{max}$, $\tilde{u}[k]$ is the actual friction force and PIVIS is in its sticking state. In contrast, if $|\tilde{u}[k]| > u_{max}$, PIVIS should be in its sliding state and the actual friction force should be equal to u_{max}. The above two statements can be combined into the following single equation (Lu *et al.* 2006)

$$u[k] = min(|\tilde{u}\,[k]|, u_{max}[k]) sgn(\tilde{u}\,[k]) \tag{23}$$

where u_{max} is defined in Eq. (20); function $\min(a, b)$ means taking the minimum value among a and b; and $sgn(\tilde{u}\,[k])$ means taking the sign of $\tilde{u}[k]$. Of note, using Eqs. (22) and (23), $u[k]$ can be computed based on only $\boldsymbol{z}[k]$ and $\ddot{z}_g[k]$. Finally, substituting the total friction $u[k]$ from Eq. (23) into Eq. (18) yields the PIVIS response $\boldsymbol{z}[k+1]$ at the next time step.

5. Control of piezoelectric friction damper

5.1 Control of PFD slip force

In dynamic Eq. (6) or Eq. (11), the PFD friction force $u_d(t)$ influenced by the embedded piezoelectric actuator can be written as

$$|u_d(t)| \le u_{d,\max}(t) = \mu_d N(t) \tag{24}$$

where $u_{d,max}$ is the slip force (maximum friction) of the PFD, μ_d is the friction coefficient of the PFD, and $N(t)$ is the controllable clamping force (normal force) generated by the embedded piezoelectric actuator. Equation (24) indicates that even though the PFD force $u_d(t)$ cannot be controlled directly, its slip force (maximum force) is a controllable quantity that can be controlled through adjustment of the clamping force $N(t)$.

To generate the controllable clamping force $N(t)$, the piezoelectric actuator has to be driven by a DC voltage supply. Fig. 6 shows a typical relationship between the normal force and the driving voltage of the PFD obtained in the experiment. As shown, the relationship can be approximated by the following linear equation (Lu *et al.* 2011c)

$$N(t) = N_0 + C_z\, V(t) \tag{25}$$

where N_0 is the initial compression force produced by the

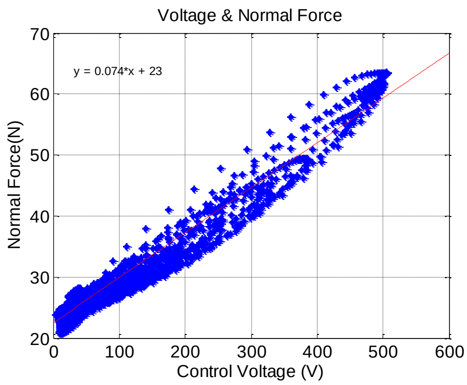

Fig. 6 Relationship between normal force and driving voltage of the PFD (N_0=23 N, C_z=0.074 N/V)

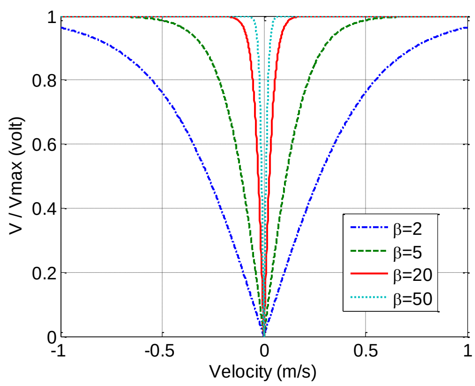

Fig. 7 Relationship between control voltage and sliding velocity for NSF controller

pre-load screw (see Fig. 4), $V(t)$ is the driving voltage of the piezoelectric actuator, and C_z is the piezoelectric coefficient (actuating force per voltage (N/V)) of the piezoelectric actuator. The value of C_z, which strongly depends on the boundary condition of the piezoelectric actuator, is usually obtained experimentally. In Fig. 6, the values of $N_0 = 23$ N and $C_z = 0.074$ N/V can be obtained from the test data using a regression method.

5.2 Non-sticking friction (NSF) control law

The determination of the control voltage $V(t)$ in Eq. (25) requires a control law. In this study, a control law called non-sticking friction (NSF) control is employed to determine the normal force of the PFD in the experiment. This control law, which requires only one sensor measurement and simple computation, is very easily implemented. The NSF controller is very efficient because it is trying to maintain the friction interface of the PFD in its sliding state (i.e., it prevents the interface from entering the sticking state) (Yang *et al.* 1987). As a result, the kinetic energy of PIVIS due to seismic excitation can be dissipated by the PFD throughout the duration of the ground motion. To achieve the goal of the NSF control law, Lu *et al.* (2011b) suggested the following formula for the driving voltage $V(t)$ of the piezoelectric actuator

$$V(t) = V_{max} tanh(\beta|\dot{z}_M(t)|) \tag{26}$$

where V_{max} denotes the voltage upper bound and β is a control sharpness parameter related to the sliding velocity $|\dot{z}_M(t)|$. Eq. (26) is the NSF voltage control law used in this study. Parameter β defines how sharply $V(t)$ varies with $|\dot{z}_M(t)|$. Fig. 7 shows the normalized voltage $V(t)/V_{max}$ as a function of the velocity $|\dot{z}_M(t)|$ for four values of β (2, 5, 20, and 50). When a higher β is adopted, the control voltage increases more rapidly from 0.0 to 1.0 as the velocity increases. The figure shows that the control voltage approaches zero whenever the PFD approaches its sticking state, i.e., $|\dot{z}_M(t)| = 0$ (the sliding velocity approaches zero). According to Eq. (26), the realization of the NSF controller requires only the feedback of the sliding velocity $|\dot{z}_M(t)|$. Moreover, substituting Eq. (26) into Eq. (25) yields the controllable clamping force of the PFD

$$N(t) = N_0 + C_z V_{max} tanh(\beta|\dot{z}_M(t)|) \tag{27}$$

The above equation indicates that the clamping force $N(t)$ varies between N_0 and $(N_0 + N_{max})$, where $N_{max} = C_z V_{max}$. Eq. (27) also states that the PFD will provide variable clamping force $N(t)$ when the PFD is in its sliding state ($|\dot{z}_M(t)| \neq 0$), whereas the PFD will only apply the minimum clamping force N_0 in its sticking state ($|\dot{z}_M(t)| = 0$). This gives the PFD a higher chance to return to its sliding state and dissipate energy.

5.3 Parametric study for NSF control parameters

Given the pre-determined N_0 and C_z, Eq. (27) indicates that the NSF control law has two control parameters, namely the maximum driving voltage V_{max} and velocity sharpness factor β. The values of these two parameters affect the control performance of PIVIS; therefore, a parametric study was conducted to find the optimal values of these parameters for the experiment. The parametric study was carried out using the numerical method described in Section 4. In this subsection, the system parameters of PIVIS and the input ground motions used in the numerical study are introduced and the results of the parametric study are discussed.

5.3.1 System parameters of PIVIS and PFD

The third column of Table 1 lists the system parameters of PIVIS used in the parametric study. These parameters, except for the NSF parameters V_{max} and β, were all identified from a pilot test conducted on the prototype PIVIS to be tested. As shown in Table 1, the ratio of moment R and the ratio of moment arm R_L of the prototype were taken to be 0.264 and 0.786, respectively. These values result in an effective frequency of $\bar{\omega} = 0.66$ Hz, which is lower than the frequency of the traditional counterpart ($\omega = 0.726$ Hz). Of note, because the PFD already provides additional damping u_d, the supplementary viscous damping c shown in Fig. 2 was not installed in the prototype system, and thus we have $\bar{\zeta} = 0$. Furthermore, to find the values of N_0 and C_z experimentally, Fig. 6 plots the normal force $N(t)$ as a function of $V(t)$ of the PFD obtained in the pilot test. As shown in Fig. 6, $N(t)$ and

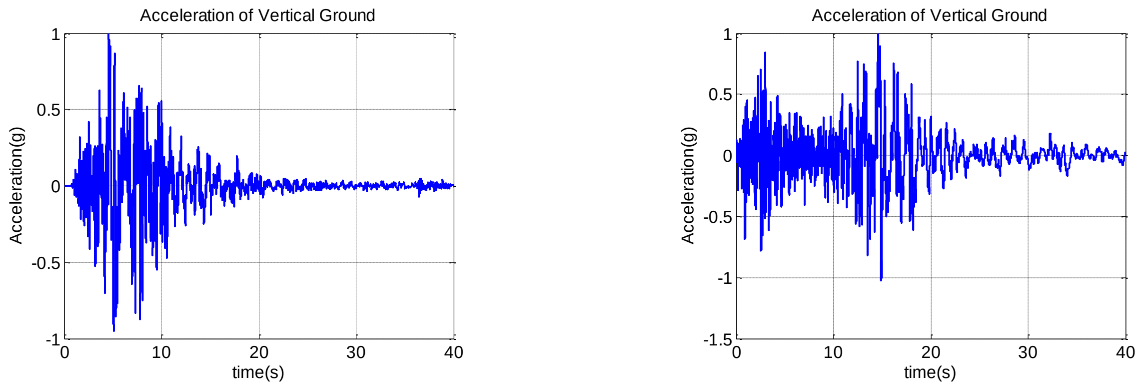

(a) Kobe (JMA)　　(b) Loma Prieta (Oakland)

Fig. 8 Ground motions for shaking table test (PGA scaled to 1.0 g)

$V(t)$ have a linear relationship that can be identified using a linear regression method. The slope of the regression line represents the piezoelectric coefficient $C_z = 0.07$ N/V, and the intersection of the line with the y-axis is equal to the pre-compression force $N_0 = 23$ N.

5.3.2 Input ground motions for parametric study

As mentioned previously, one of the advantages of using PIVIS is to mitigate the resonance-like response incurred in a near-fault earthquake with long-period components. Two vertical ground motions with near-fault characteristics were

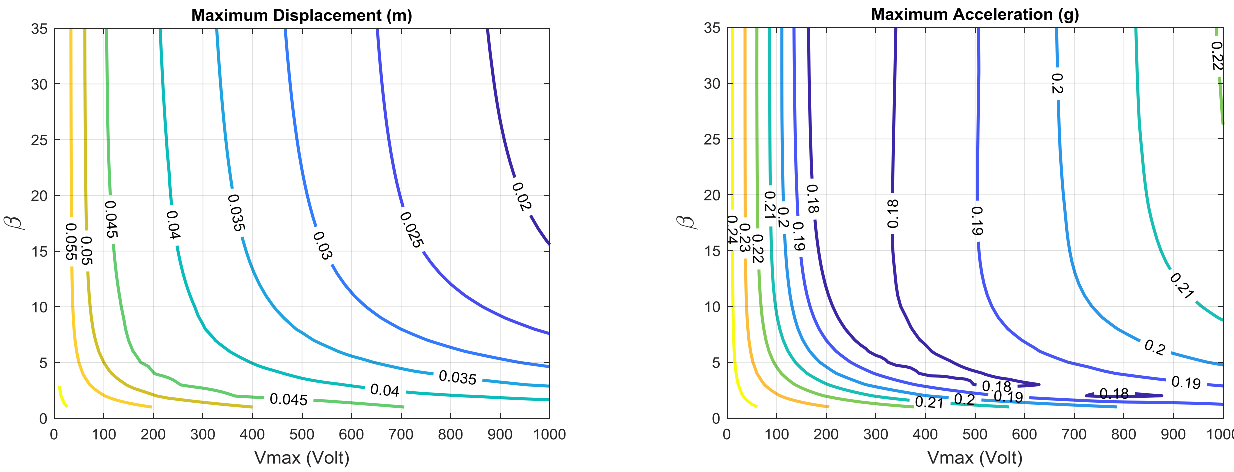

(a) Isolation displacement　　(b) Equipment acceleration

Fig. 9 Peak responses of PIVIS for various β and V_{max} (Kobe (JMA), PGA = 0.3 g)

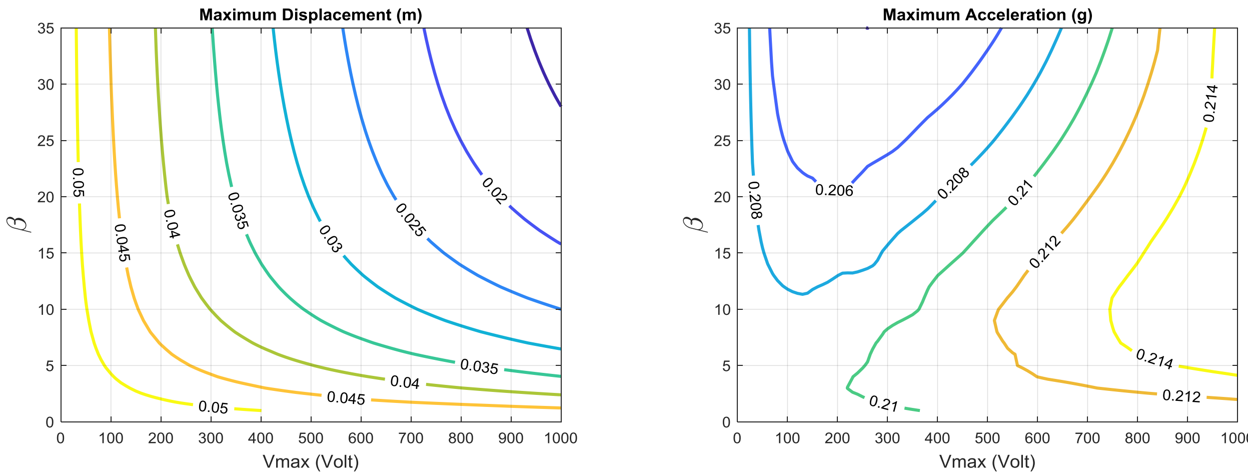

(a) Isolation displacement　　(b) Equipment acceleration

Fig. 10 Peak responses of PIVIS for various β and V_{max} ((Loma Prieta (Oakland), PGA = 0.3 g) thus chosen for the parametric study, namely the Kobe earthquake (JMA Station 1995) and the Loma Prieta earthquake (Oakland Station, USA, 1989). Figs. 8(a) and (b) show the time histories of the vertical components of the Kobe and Loma Prieta earthquakes, respectively. In the figures, the vertical peak ground acceleration (PGA) of both records is normalized to 1.0 g.

5.3.3 Results of parametric study

To find the best values of the control parameters β and V_{max}, the contour plots in Figs. 9 and 10 show the peak responses of PIVIS for various combinations of β and V_{max} under the vertical components of the Kobe and Loma Prieta earthquakes, respectively. The PGA of both ground motions is scaled to 0.3 g. The subplots (a) and (b) in each figure show the peak isolation displacement and peak acceleration of the isolated equipment, respectively. From Figs. 9 and 10, the following observations can be made. (1) As shown in Figs. 9(a) and 10(a), the isolation displacement of PIVIS decreases when β or V_{max} increases. When β is larger than 20, the isolation displacement becomes insensitive to the change in β. (2) The equipment acceleration increases when a smaller V_{max} is applied. This is due to insufficient controllable force u_d provided by the PFD. However, the equipment acceleration also increases when a larger V_{max} is applied. (3) In Fig. 9(b), the lowest equipment acceleration can be obtained when β is between 10 and 35 and V_{max} is between 200 and 500 V. Moreover, in Fig. 10(b), the lowest equipment acceleration can be obtained when β is between 20 and 35 and V_{max} is between 100 and 500 V. (4) Considering the control effectiveness of both isolation displacement and equipment acceleration, $\beta = 20$ and $V_{max} = 500\,V$ were chosen as the parameters for the NSF controller for the shaking table test.

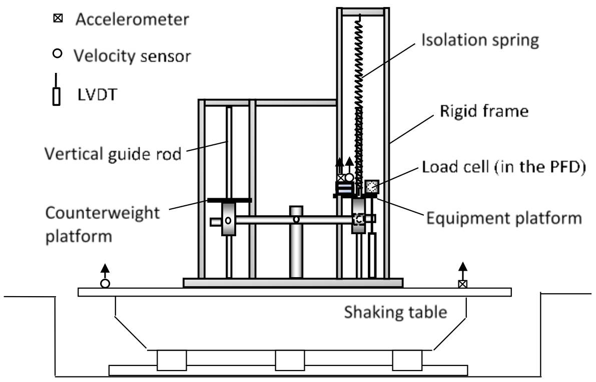

Fig. 11 Sensor placements of shaking table test

6. Experimental verification of PIVIS by shaking table test

6.1 Test setup

Fig. 11 shows the setup and instrumentation of the shaking table test conducted for the prototype PIVIS. The system parameters of the tested prototype are listed in the third column of Table 1. As shown in Fig. 11, a linear variable differential transformer (LVDT), a velocity meter, and an accelerometer were placed on the equipment platform to measure the responses of the equipment isolated by PIVIS. Moreover, a velocity meter and an accelerometer were also mounted on the shaking table to record the generated ground acceleration, which is used as the input excitation in the later numerical simulation. Furthermore, a load cell was installed in the PFD (see Fig. 4) to measure the controllable normal force generated by the piezoelectric actuator. The vertical components of the Kobe and Loma Prieta earthquakes were used as the input ground motions.

Table 1 Parameters of various isolation systems used for numerical simulation

Component	Item	PIVIS	Passive[(1)]	Traditional
Vertical isolation system	Mass of equipment (M)	16 kg	16 kg	16 kg
	Isolation stiffness (k)	336 N/m	336 N/m	336 N/m
	Traditional period (T)	1.377 s	1.377 s	1.377 s
	Traditional frequency (ω)	0.726 Hz	0.726 Hz	0.726 Hz
	Inherent friction (u_i)	3.87 N	3.87 N	3.87 N
Counterweight and leverage mechanism	Counterweight (m)	5.374 kg	5.374 kg	--
	Ratio of moment (R)	0.264	0.264	--
	Ratio of moment arm (R_L)	0.786	0.786	--
	Effective frequency ($\bar{\omega}$)	0.66 Hz	0.66 Hz	--
	Effective period ($\bar{T}$)	1.513 s	1.513s	--
Piezoelectric friction damper (PFD)	Friction coefficient (μ_d)	0.15	--	--
	Piezoelectric coefficient (C_z)	0.074 N/V	--	--
	Pre-compression (N_0)	23 N	--	--
NSF Controller	Maximum voltage (V_{max})	500 V	--	--
	Velocity coefficient (β)	20	--	--

(1) Passive system means passive-PIVIS in which the PFD is completely removed from PIVIS

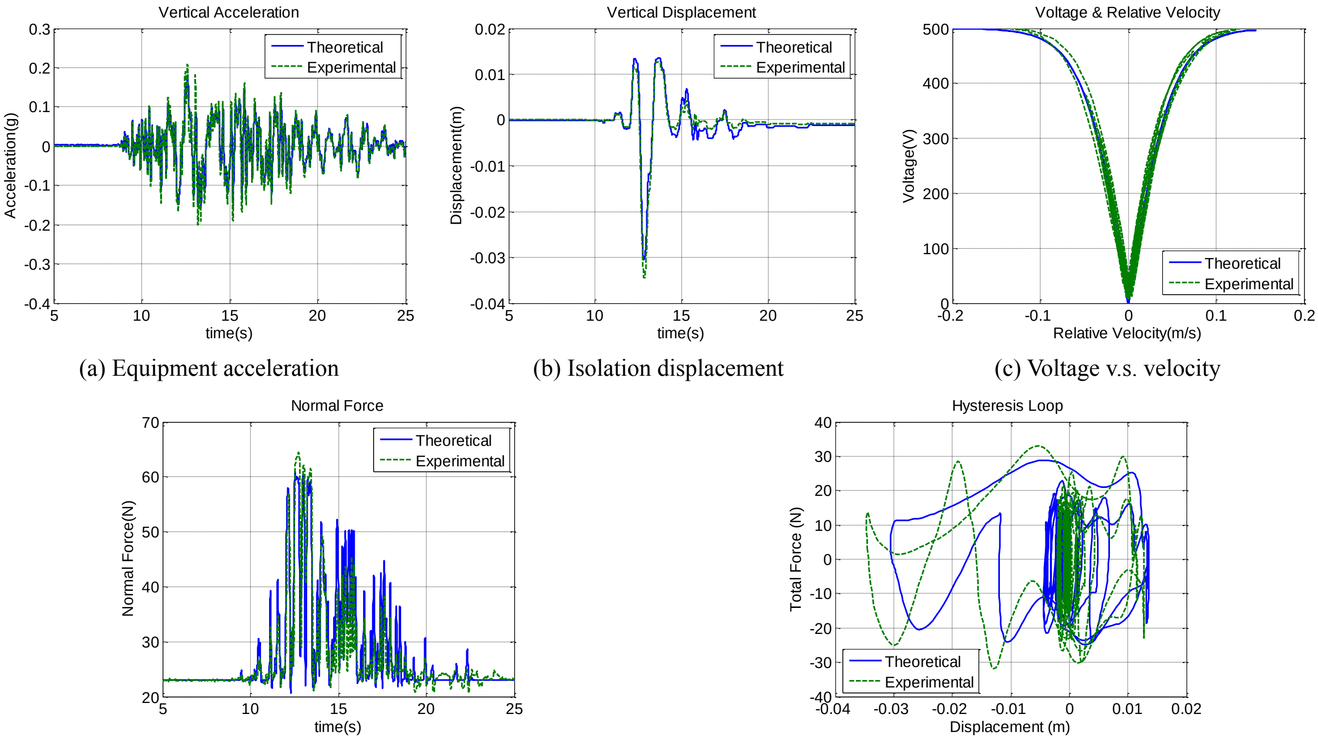

(a) Equipment acceleration (b) Isolation displacement (c) Voltage v.s. velocity

(d) Normal force (e) Hysteresis loop

Fig. 12 Comparison of theoretical and experimental results of PIVIS (Kobe, PGA = 0.35 g)

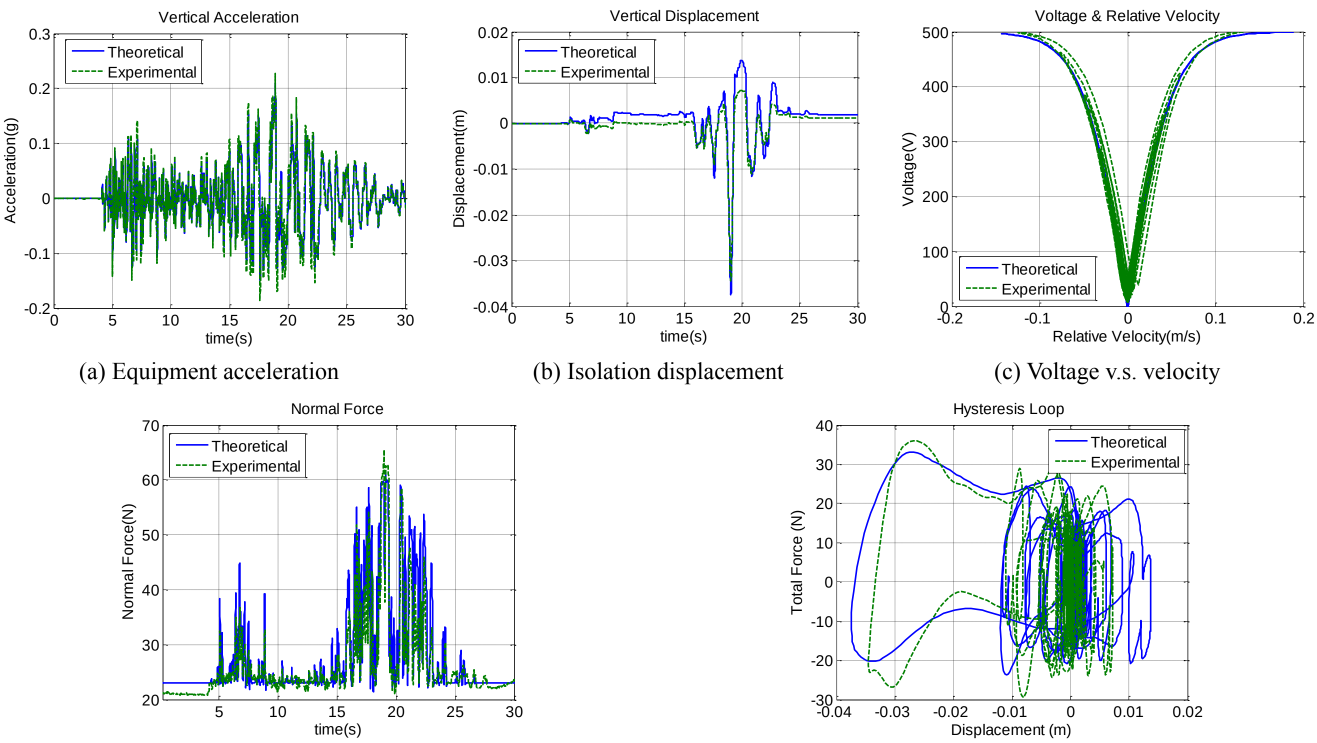

(a) Equipment acceleration (b) Isolation displacement (c) Voltage v.s. velocity

(d) Normal force (e) Hysteresis loop

Fig. 13 Comparison of theoretical and experimental results of PIVIS (Loma Prieta, PGA = 0.35 g)

Notably, the piezoelectric actuator in the PFD usually requires a DC electric power of high voltage but low current. The DC voltage, which may go up to 500 V or more, is usually provided by a voltage amplifier. In the experiment of this study, an amplifier with a gain of 100 V/V to amplify a 5 V control signal to a driving voltage of 500 V. On the other hand, the electric current required for the piezoelectric actuator is usually at a range of several mA, so the total energy demand to control the piezoelectric actuator is actually minimal, and may be provided by a battery system.

6.2 Comparison of experimental and theoretical results

To experimentally verify the developed PIVIS analysis method, the simulated theoretical responses of PIVIS due to the Kobe and Loma Prieta earthquakes are compared with the experimental responses in Figs. 12 and 13, respectively. There are five subplots in each of these figures. The subplots represent (a) the time response of the equipment acceleration, (b) the time response of isolation displacement, (c) the control voltage as a function of sliding velocity, (d) the time response of the PFD clamping (normal) force, and (e) the hysteresis loop of PIVIS. In each subplot, the solid and dotted lines represent the numerical and experimental results, respectively. In both Figs. 12(e) and 13(e), the force in the hysteresis loop is estimated as

$$F_z(t) = M\ddot{z}_{M,exp} \tag{28}$$

where F_z represents the total vertical force applied to the isolated equipment by PIVIS and $\ddot{z}_{M,exp}$ denotes the equipment acceleration measured in the experiment.

The following observations can be made from Figs. 12 and 13. (1) In general, the simulation results well agree with the experimental ones in both time responses and hysteresis loops. (2) Subplots (c) and (d) demonstrate that the control voltage and the clamping force of the PFD can be adjusted in a desired manner, verifying the controllability of the PFD. (3) Subplots (e) show that due to the reactive force f_M resulting from the inertial force of the counterweight (see Fig. 2), the shape of the PIVIS hysteresis loop becomes irregular. This shape is very different from that of a conventional isolation system shown in Fig. 1. This reactive force may help suppress the vibration of equipment. (4) Some deviations between the theoretical and experimental results can be observed in subplots (b) and (e). One reason for the deviations is the neglect of the moment of inertia of the lever arm in the dynamic equation (see Eq. (6)).

7. Evaluation of isolation performance of PIVIS by numerical simulation

In this study, the experimental results of the PIVIS are mainly used to verify the mathematic model and its corresponding dynamic equation and not to demonstrate the isolation performance. However, since the magnitude and frequency content of the input ground motions may affect the behavior of PIVIS, to fully investigate the isolation performance of PIVIS in earthquakes with various characteristics, in this section, the responses of PIVIS subjected to 14 different vertical ground motions with various PGA levels are simulated. For comparison, the responses of PIVIS in semi-active mode are compared with those of PIVIS in passive mode (passive PIVIS) and those of its traditional counterpart system (traditional system). In passive PIVIS, the PFD is removed from PIVIS (i.e., $u_d = 0$ in Fig. 2) but the leverage mechanism and counterweight are retained. In the traditional system (see Fig. 1), the PFD and leverage mechanism are removed from PIVIS. The system parameters for the three systems (i.e., PIVIS, passive PIVIS and traditional VIS) are listed in Table 1.

There are two reasons that the responses of PIVIS in semi-active and passive modes were compared by using the numerically simulated results instead of experimental results. Firstly, in order to compare the isolation performance of the PIVIS in passive and semi-active modes more thoroughly, 14 ground motions including 7 near-fault ground motions that contain strong long-period components will be considered. To reproduce a near-fault ground

Table 2 Average of response spectra for each of the 14 selected vertical ground motions

Characteristic	Earthquake (station)	Average spectral acceleration[(1)] (g)	Average spectral displacement[(1)] (m)
Far-field earthquake	1994 Northridge (Newhall)	0.143	0.197
	1940 El Centro	0.165	0.228
	1994 Northridge (Sylmar)	0.203	0.287
	1994 Northridge (Lacc North)	0.422	0.559
	1992 Landers (Yermo)	0.426	0.464
	1989 Loma Prieta (Hollister)	0.506	0.872
	1992 Cape Mendocino (Petrolia)	0.537	0.855
Near-fault earthquake	1995 Kobe (JMA)	0.613	0.591
	1989 Loma Prieta (Lexington)	0.658	0.816
	1989 Loma Prieta (Oakland)	0.696	0.715
	1999 Chi-Chi (TCU068)	0.969	1.710
	1999 Chi-Chi (TCU075)	1.008	1.694
	1999 Chi-Chi (TCU052)	1.296	2.238
	1999 Chi-Chi (TCU102)	1.516	2.326

[(1)] The average of spectral value is taken for the period between 1.0 to 4.0 s

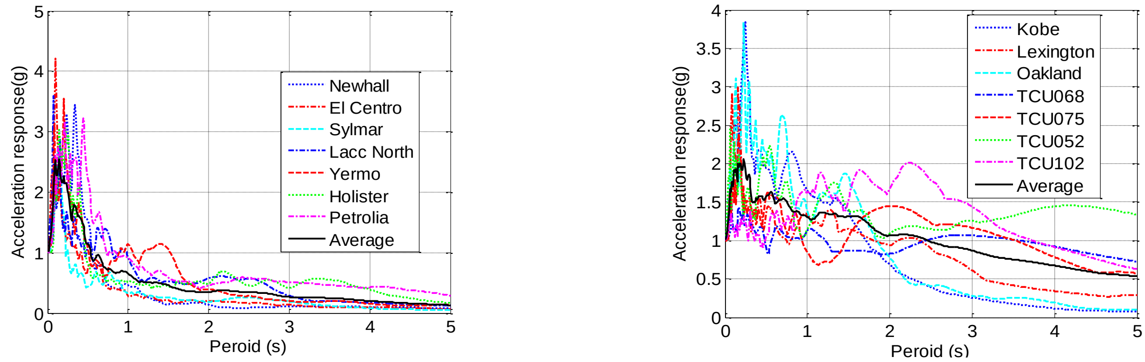

(a) Seven far-field earthquakes (b) Seven near-fault earthquakes

Fig. 14 Acceleration response spectra of fourteen vertical ground motions

accelerations in a test generally requires a very long-stroke shaking table. Due to the stroke limit, the shaking table used in this study could not generate some of the near-fault ground motions with a higher intensity. Secondly, it is very difficult for a shaking table to generate two exactly same vertical ground accelerations for the passive and semi-active systems; therefore, an accurate comparison between the two systems would be difficult to achieve by the test.

7.1 Selected ground accelerations

Fourteen vertical ground motions, including seven near-fault earthquakes and seven far-field earthquakes, are considered in the numerical simulation. Table 2 lists these ground motions. The classification of near-fault and far-field earthquakes is based on the average values of displacement and acceleration spectra in the structural period of 1 to 4 s. As shown in Table 2, for a specific ground motion, if the average of the spectral displacement for the structural periods of 1 to 4 s is larger than 0.5 m and at the same time the average of the spectral acceleration is larger than 0.6g, the ground motion is classified as a near-field earthquake; otherwise, the ground motion is classified as a far-field earthquake. Figs. 14(a) and (b) compare the acceleration response spectra for the seven far-field and seven near-fault earthquakes, respectively. The solid line in the figures represents the average response spectrum curve. From Fig. 14, it is observed that the spectral accelerations of the seven near-fault earthquakes in the long-period range (1-4 s) are higher than those of the seven far-field earthquakes. This implies that the near-fault earthquakes tend to induce larger responses for a long-period system such as a seismic isolation system.

7.2 Comparison with traditional isolation system

To compare the isolation performance of PIVIS (with NSF) and the traditional system in the time domain, a representative near-fault earthquake (Kobe) and a far-field earthquake (El Centro) are considered as the input ground motion in Figs. 15 and 16, respectively. In these figures, the PGA of both vertical ground motions is scaled to 0.4g, and the isolation displacement, equipment acceleration, and hysteresis loop of PIVIS and the traditional system are compared. Figs. 15(a) and (b) show that under the excitation of the near-fault Kobe earthquake, the traditional system exhibits resonance-like behavior and a severe oscillation response, whereas PIVIS very effectively suppresses this oscillation and prevents the resonance response. Fig. 15(c) shows that the typical shape of the hysteresis loop (parallelogram) is obtained for the traditional isolation system, and that an irregular shape of the hysteresis loop is obtained for PIVIS (due to reactive force f_M resulting from the counterweight). This reactive force and the friction force u_d of the PFD effectively suppress the motion of the equipment isolated by PIVIS.

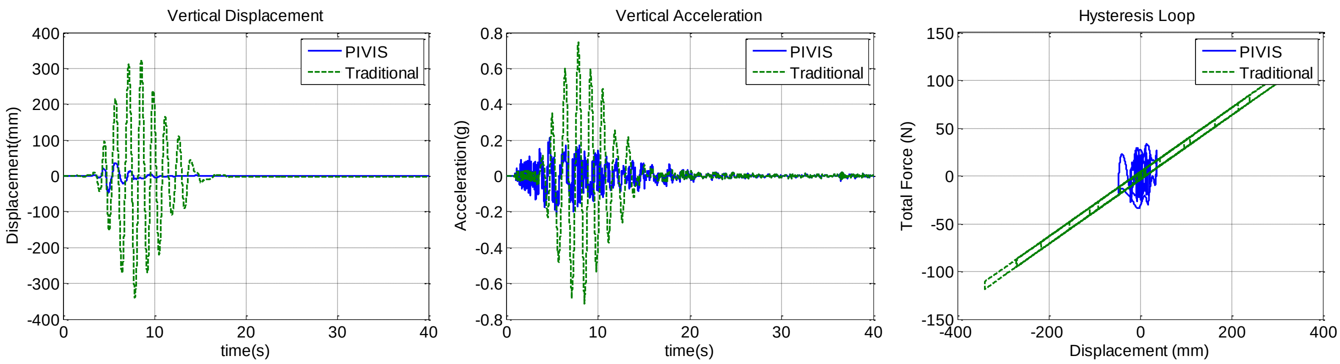

(a) Isolation displacement (b) Equipment acceleration (c) Hysteresis loop

Fig. 15 Responses of PIVIS and traditional system (Kobe, PGA = 0.4 g)

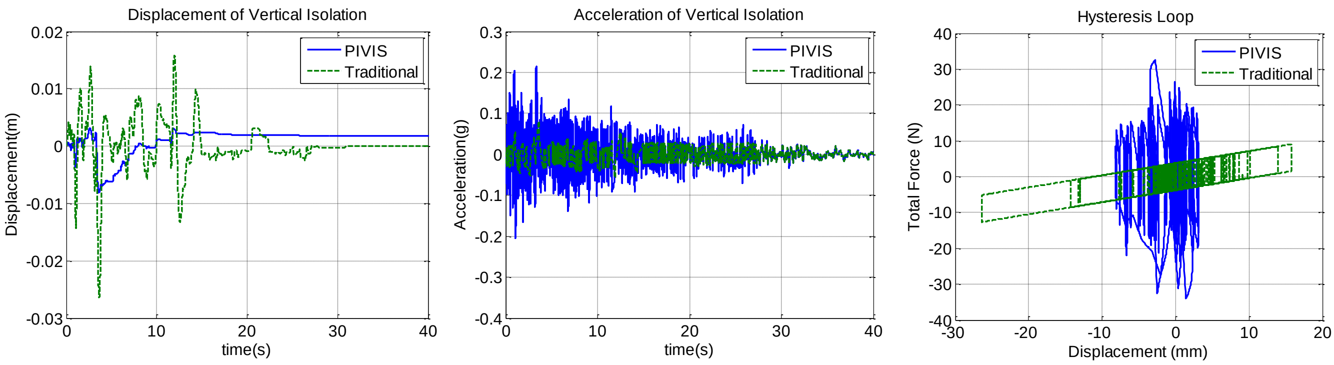

(a) Isolation displacement (b) Equipment acceleration (c) Hysteresis loop

Fig. 16 Responses of PIVIS and traditional system (El Centro, PGA = 0.4 g)

Table 3 Comparison of average peak responses of PIVIS (with NSF) and traditional system under different earthquakes

Earthquake type	(a) PGA (g)	Ave. peak isolation displacement			Ave. peak equipment acceleration			
		(b) Traditional (mm)	(c) PIVIS (mm)	(c)/(b) Ratio(1)	(d) Traditional (g)	(d)/(a) Ratio(2)	(e) PIVIS (g)	(e)/(a) Ratio(2)
Near-fault (7 records)	0.1	36.7	2.18	0.060	0.101	1.01	0.085	0.846
	0.2	119	20.0	0.171	0.276	1.38	0.153	0.763
	0.3	210	50.3	0.239	0.470	1.57	0.225	0.751
	0.4	303	91.4	0.302	0.665	1.66	0.311	0.778
	0.5	402	137	0.342	0.877	1.75	0.413	0.825
		Average		**0.223**	**Average**	**1.47**	**Average**	**0.793**
Far-field (7 records)	0.1	4.45	0.364	0.082	0.033	0.330	0.081	0.813
	0.2	38.5	3.49	0.091	0.105	0.200	0.130	0.650
	0.3	51.4	6.13	0.119	0.133	0.442	0.173	0.578
	0.4	81.2	12.0	0.147	0.196	0.490	0.217	0.541
	0.5	117	20.1	0.172	0.271	0.542	0.260	0.519
		Average		**0.122**	**Average**	**0.401**	**Average**	**0.620**
Total (14 records)	0.1	20.6	1.27	0.062	0.067	0.672	0.083	0.829
	0.2	71.8	11.4	0.159	0.176	0.879	0.141	0.706
	0.3	131	28.2	0.216	0.301	1.00	0.199	0.664
	0.4	192	51.7	0.269	0.430	1.08	0.264	0.660
	0.5	260	78.8	0.304	0.574	1.16	0.336	0.672
		Average		**0.202**	**Average**	**0.958**	**Average**	**0.706**

(1) The peak displacement of the PIVIS (NSF) divided by that of the traditional system
(2) The peak acceleration of the PIVIS (NSF) or traditional system divided by the PGA

For the far-field El Centro earthquake, which contains more high-frequency content, Fig. 16 shows that PIVIS has less isolation displacement but has a higher acceleration response compared with those for the traditional system. Nevertheless, the peak acceleration of PIVIS is only about 0.2 g, which is only half of PGA (0.4 g). This indicates that for far-field earthquakes, the isolation efficiency of PIVIS is preserved even though it is not as efficient as the traditional system.

To further evaluate the isolation performance of PIVIS with more ground motions, Table 3 compares the average peak responses of PIVIS (with NSF) and the traditional systems under the 14 chosen earthquakes with five different PGA levels. It is shown the average of the peak isolation displacements of PIVIS is lower than that of the traditional system for both near-fault and far-field earthquakes. Considering all 14 earthquakes, the average of the PIVIS displacement is only about 20% of that of the traditional system. In other words, PIVIS reduces isolator displacement by 80%, and thus greatly reduces the required isolation space. For the equipment acceleration response, Table 3 shows that the traditional system has excellent

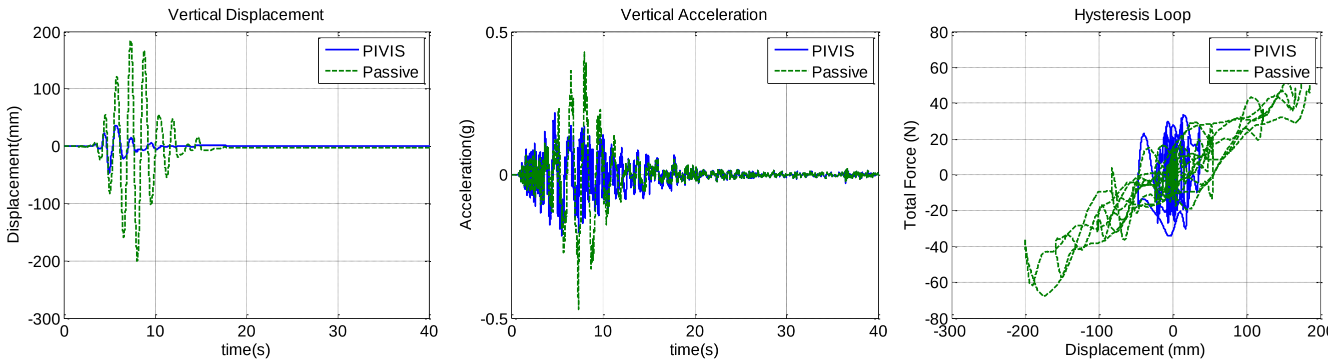

(a) Isolation displacement (b) Equipment acceleration (c) Hysteresis loop

Fig. 17 Responses of PIVIS and the passive PIVIS (Kobe, PGA = 0.4 g)

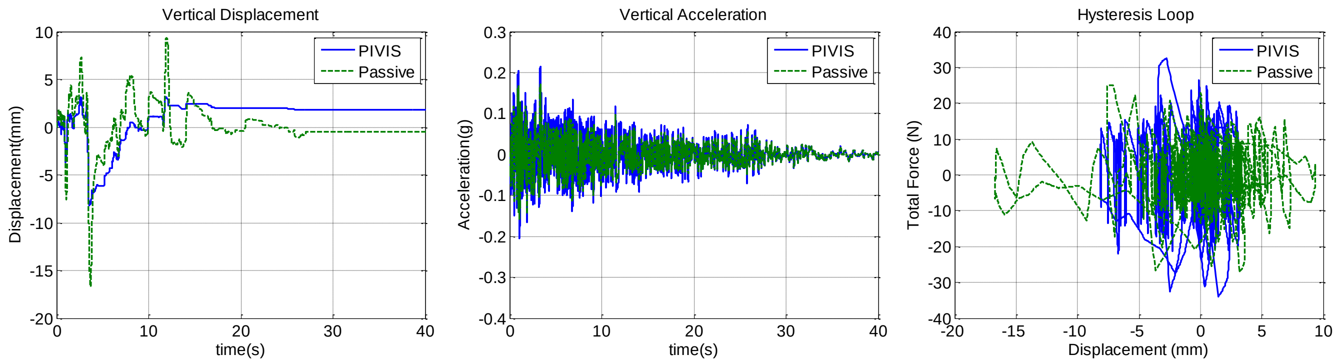

(a) Isolation displacement (b) Equipment acceleration (c) Hysteresis loop

Fig. 18 Responses of PIVIS and passive PIVIS (El Centro, PGA = 0.4 g)

isolation performance under the seven far-field earthquakes, for which it reduces the peak acceleration to about 40% of PGA. However, the traditional system performs poorly for the seven near-fault earthquakes, for which its average peak acceleration is amplified to about 1.47 times PGA. In contrast, PIVIS reduces the peak acceleration to about 80% and 60% of PGA for the near-fault and far-field earthquakes, respectively. This shows that PIVIS can prevent the resonant behavior induced by a near-fault earthquake, which usually has strong long-period components. Therefore, unlike the traditional system, PIVIS is an effective isolation system for both earthquake type.

7.3 Comparison with passive PIVIS

Similar to Figs. 15 and 16, Figs. 17 and 18 compare the simulated responses of PIVIS (with NSF) and passive PIVIS ($u_d = 0$) under the Kobe and El Centro earthquakes, respectively. Fig. 17 shows that the passive system exhibits resonance-like behavior for the near-fault Kobe earthquake, although the amplitude of the oscillation is reduced compared with that of the traditional system shown in Fig. 15. Fig. 17 also shows that this resonance-like response is effectively mitigated by the PFD in PIVIS (with NSF control law). For the far-field El Centro earthquake, Fig. 18 shows that PIVIS has a lower peak isolation displacement than that of the passive system, and that the peak equipment accelerations of both systems are at the same level. This indicates that the PFD in PIVIS can reduce isolation displacement while maintaining isolation efficiency. Figs. 17 and 18 show that in both far-field and near-fault earthquakes, PIVIS with the NSF controller exhibits better isolation performance than that of passive PIVIS.

For the fourteen selected earthquakes with five different PGA levels, Table 4 compares the average peak responses of PIVIS and the passive system. As shown in the table, for both near-fault and far-field ground motions, the peak isolation displacement of PIVIS is always lower than that of passive PIVIS. When all fourteen earthquakes are considered, the average peak displacement of PIVIS is only about 32.7% of that of passive PIVIS. Regarding the equipment acceleration response, the peak acceleration of PIVIS is much lower than that of passive PIVIS for the seven near-fault earthquakes, even though PIVIS has a slightly higher acceleration for the seven far-field earthquakes, for which PIVIS is still an effective isolation system because it reduces the average peak acceleration to about 62% of PGA. When all fourteen earthquakes are considered, Table 4 shows that the average peak acceleration of PIVIS is only 70.6% of PGA, which is lower than that of passive PIVIS (76.1%). This demonstrates that, compared with the passive system, PIVIS with the NSF control law has better isolation performance in terms of displacement and acceleration responses.

Table 4 Comparison of average peak responses of PIVIS (with NSF) and passive PIVIS under different earthquakes

Earthquake type	(a) PGA (g)	Ave. peak isolation displacement			Ave. peak equipment acceleration			
		(b) Passive (mm)	(c) PIVIS (mm)	(c)/(b) Ratio[(1)]	(d) Passive (g)	(d)/(a) Ratio[(2)]	(e) PIVIS (g)	(e)/(a) Ratio[(2)]
Near-fault (7 records)	0.1	18.1	2.18	0.121	0.076	0.761	0.085	0.846
	0.2	69.7	20.4	0.293	0.184	0.918	0.153	0.763
	0.3	138	50.3	0.365	0.315	1.05	0.225	0.751
	0.4	205	91.4	0.445	0.450	1.13	0.311	0.778
	0.5	271	138	0.508	0.583	1.17	0.413	0.825
		Average		**0.346**	**Average**	**1.01**	**Average**	**0.793**
Far-field (7 records)	0.1	1.71	0.364	0.213	0.061	0.606	0.081	0.813
	0.2	10.4	2.47	0.237	0.102	0.508	0.130	0.650
	0.3	26.5	6.13	0.231	0.144	0.479	0.173	0.578
	0.4	45.9	12.0	0.260	0.196	0.491	0.217	0.541
	0.5	65.8	20.1	0.305	0.255	0.510	0.260	0.519
		Average		**0.249**	**Average**	**0.519**	**Average**	**0.620**
Total (14 records)	0.1	9.90	1.27	0.129	0.068	0.684	0.083	0.829
	0.2	40.1	11.4	0.285	0.143	0.713	0.141	0.706
	0.3	82.2	28.2	0.343	0.229	0.764	0.199	0.664
	0.4	126	51.8	0.411	0.323	0.808	0.264	0.660
	0.5	168	78.8	0.468	0.419	0.838	0.336	0.672
		Average		**0.327**	**Average**	**0.761**	**Average**	**0.706**

[(1)] The peak displacement of the PIVIS (NSF) divided by that of the Passive-PIVIS system
[(2)] The peak acceleration of the PIVIS (NSF) or the Passive-PIVIS system divided by the PGA

8. Conclusions

In this paper, a semi-active isolation system called the piezoelectric inertia-type vertical isolation system (PIVIS) was proposed for the seismic protection of equipment and its isolation theory was developed. PIVIS mainly consists of a counterweight, a leverage mechanism, and a piezoelectric friction damper (PFD). The leverage mechanism transfers the gravitational and inertial forces generated by the counterweight to the equipment side, and thus provides an additional reactive force to the isolated equipment. Consequently, in the static state, PIVIS can prevent excessive initial settlement of the isolation system due to the self-weight of the equipment, and in the dynamic state, the counterweight and the leverage mechanism lengthen the effective isolation period. The PFD with a suitable control law provides a controllable friction force to PIVIS, suppressing excessive isolation displacement induced by a near-fault earthquake with long-period components. To verify the feasibility of PIVIS, a prototype PIVIS was manufactured and tested dynamically using a shaking table. In the test, a simple semi-active control law called NSF control was employed. Using fourteen vertical ground motions, including seven near-fault and seven far-field earthquakes, with five different PGA levels, the peak responses of PIVIS were simulated and compared with those of a counterpart traditional isolation system and passive PIVIS.

Based on the experimental and numerically simulated results, the following conclusions were obtained. (1) The results of the shaking table test well agree with the theoretical results. This verifies the feasibility of PIVIS and the correctness of the developed theoretical model and numerical method for predicting the dynamic response of PIVIS. (2) For the fourteen selected vertical ground motions, the numerical results show that the average peak isolation displacement of semi-active PIVIS is only about 20% and 33% of those of the traditional and passive systems, respectively. This demonstrates that PIVIS with a controllable friction force can effectively suppress isolation displacement and greatly reduce the required isolation space. (3) In terms of mitigating equipment acceleration, the traditional system performs very poorly for near-fault earthquakes with strong long-period components; the average peak acceleration is amplified up to about 147% of PGA due to a resonance-like response. In contrast, PIVIS reduces the peak acceleration response to about 79% of PGA on average. (4) For far-field earthquakes, the peak acceleration response of PIVIS may be slightly higher than those of the traditional and passive systems; however, PIVIS is still a very effective isolation system because its average peak acceleration is much lower than PGA.

Acknowledgments

This research was supported in part by the Ministry of Science and Technology of R.O.C. (Taiwan) through grant MOST108-2625-M-006-005. The authors are grateful to the National Center for Research on Earthquake Engineering (NCREE, Taipei) for its technical support of the experiment.

References

Araki, Y., Asai, T. and Masui, T. (2011), "Response of vibration-isolated object to ground motions with intense vertical accelerations", *Eng. Struct.*, **33**(12), 3610-3619. https://doi.org/10.1016/j.engstruct.2011.07.025

Araki, Y., Asai, T., Kimura, K., Maezawa, K. and Masui, T. (2013), "Nonlinear vibration isolator with adjustable restoring force", *J. Sound Vib.*, **332**(23), 6063-6077. https://doi.org/10.1016/j.jsv.2013.06.030

Asai, T., Araki, Y., Kimura, K. and Masui, T. (2017), "Adjustable vertical vibration isolator with a variable ellipse curve mechanism", *Earthq. Eng. Struct. Dyn.*, **46**(8), 1345-1366. https://doi.org/10.1002/eqe.2859

Badalouka, B.G. and Papadopoulos, G.A. (2008), "Experimental study of a structure under stress pulse simulating vertical ground motion", *J. Earthq. Eng.*, **12**(3), 341-356. https://doi.org/10.1080/13632460701457017

Chang, C.M., Spencer, B.F. and Shi, P. (2014), "Multiaxial active isolation for seismic protection of buildings", *Struct. Control Health Monitor.*, **21**(4), 484-502. https://doi.org/10.1002/stc.1579

Chu, S.Y., Lu, L.Y. and Yeh, S.W. (2018), "Real-time hybrid testing of a structure with a piezoelectric friction controllable mass damper by using a shake table", *Struct. Control Health Monitor.*, **25**(3), e2124. https://doi.org/10.1002/stc.2124

FEMA (2011), Reducing the risks of nonstructural earthquake damage - A practical guide. Report no. FEMA E-74, Federal Emergency Management Agency, Washington, D.C, USA.

Franke, D., Lam, N., Gad, E. and Chandler, A. (2005), "Seismically induced overturning of objects and filtering effects of buildings", *JSEE: Summer*, **7**(2), 95-108.

Fujita, S. (1996), "Shake table tests on three-dimensional vibration isolation system comprising rubber bearing and coil springs", *Proceedings of the 11th World Conference on Earthquake Engineering*, No.276, Acapulco, Mexico, June.

Furukawa, S., Sato, E., Shi Y., Becker, T. and Nakashima, M. (2013), "Full-scale shaking table test of a base-isolated medical facility subjected to vertical motions", *Earthq. Eng. Struct. Dyn.*, **42**(13), 1931-1949. https://doi.org/10.1002/eqe.2305

Jangid, R.S. and Kelly, J.M. (2001), "Base isolation for near-fault motion", *Earthq. Eng. Struct. Dyn.*, **30**(5), 691-707. https://doi.org/10.1002/eqe.31

Kitamura, S., Okamura, S. and Takahashi, K. (2005), "Experimental study on vertical component seismic isolation system with coned disk spring", *ASME Pressure Vessels and Piping Division Conference*, Paper No. PVP2005-71356, pp. 175-182.

Konstantinidis, D. and Makris, N. (2005), "Experimental and analytical studies on the seismic response of freestanding and anchored laboratory equipment", Report No. PEER 2005/07, Pacific Earthquake Engineering Research Center, University of California, Berkeley, CA, USA.

Konstantinidis, D. and Makris, N. (2009), "Experimental and analytical studies on the response of freestanding laboratory equipment to earthquake shaking", *Earthq. Eng. Struct. Dyn.*, **38**(6), 827-848. https://doi.org/10.1002/eqe.871

Li, X., Dou, H. and Zhu, X. (2007), "Engineering characteristics of near-fault vertical ground motions and their effect on the seismic response of bridges", *Earthq. Eng. Eng. Vib.*, **6**(4), 345-350. https://doi.org/10.1007/s11803-007-0723-5

Lin, T.K., Lu, L.Y. and Chang, H. (2015), "Fuzzy logic control of a stiffness-adaptable seismic isolation system", *Struct. Control Health Monitor.*, **22**(1), 177-195. https://doi.org/10.1002/stc.1667

Lin, T.K., Lu, L.Y. and Chen, C.J. (2018) "Semi-active leverage-type isolation system considering minimum structural energy", *Smart Struct. Syst., Int. J.*, **21**(3), 373-387. https://doi.org/10.12989/sss.2018.21.3.373

Lu, L.Y., Chung, L.L., Wu, L.Y. and Lin, G.L. (2006), "Dynamic analysis of structures with friction devices using discrete-time state-space formulation", *Comput. Struct.*, **84**(15-16), 1049-1071. https://doi.org/10.1016/j.compstruc.2005.12.005

Lu, L.Y., Lee, T.Y. and Yeh, S.W. (2011a), "Theory and experimental study for sliding isolators with variable curvature", *Earthq. Eng. Struct. Dyn.*, **40**(14), 1609-1627. https://doi.org/10.1002/eqe.1106

Lu, L.Y., Lin, G.L. and Lin, C.Y. (2011b), "Experiment of an ABS-type control strategy for semi-active friction isolation systems", *Smart Struct. Syst., Int. J.*, **8**(5), 501-524. https://doi.org/10.12989/sss.2011.8.5.501

Lu, L.Y., Lin, G.L. and Lin, C.Y. (2011c), "Experimental verification of a piezoelectric smart isolation system", *Struct. Control Health Monitor.*, **18**(8), 869-889. https://doi.org/10.1002/stc.407

Lu, L.Y., Chu, S.Y., Yeh, S.W. and Chung, L.L. (2012), "Seismic test of least-input-energy control with ground velocity feedback for variable-stiffness isolation systems", *J. Sound Vib.*, **331**(4), 767-784. https://doi.org/10.1016/j.jsv.2011.10.012

Lu, L.Y., Lin, C.C. and Lin, G.L. (2013a), "Experimental evaluation of supplemental viscous damping for a sliding isolation system under pulse-like base excitation", *J. Sound Vib.*, **332**(8), 1982-1999. https://doi.org/10.1016/j.jsv.2012.12.008

Lu, L.Y., Lee, T.Y., Juang, S.Y. and Yeh, S.W. (2013b), "Polynomial friction pendulum isolators (PFPIs) for building floor isolation: An experimental and theoretical study", *Eng. Struct.*, **56**(2013), 970-982. https://doi.org/10.1016/j.engstruct.2013. 06.016

Lu, L.Y., Chen, P.R. and Pong, K.W. (2016), "Theory and experiment of an inertia-type vertical isolation system for seismic protection of equipment", *J. Sound Vib.*, **366**, 44-61. https://doi.org/10.1016/j.jsv.2015.12.009

Makris, N. and Chang, S.P. (2000), "Effect of viscous, visco-plastic and friction damping on the response of seismic isolated structures", *Earthq. Eng. Struct. Dyn.*, **29**(1), 85-107. https://doi.org/10.1002/(SICI)1096-9845(200001)29:1<85::AID-EQE902>3.0.CO;2-N

Memari, A.M., Maneetes, H. and Bozorgnia, Y. (2004), "Study of the effect of near-source vertical ground motion on seismic design of precast concrete cladding panels", *J. Architect. Eng.*, **10**(4), 167-184. https://doi.org/10.1061/(ASCE)1076-0431(2004)10:4(167)

Murnal, P. and Sinha, R. (2004), "Aseismic design of structure–equipment systems using variable frequency pendulum isolator", *Nuclear Eng. Des.*, **231**(2), 129-139. https://doi.org/10.1016/j.nucengdes.2004.03.009

Narasimhan, S. and Nagarajaiah, S. (2005), "A STFT semi-active controller for base isolated buildings with variable stiffness isolation systems", *Eng. Struct.*, **27**(4), 514-523. https://doi.org/10.1016/j.engstruct.2004.11.010

Narasimhan, S., Nagarajaiah, S., Johnson, E.A. and Gavin, H.P. (2006), "Smart base-isolated benchmark building. Part I:

problem definition", *Struct. Control Health Monitor.*, **13**(2-3), 573-588. https://doi.org/10.1002/stc.99

Papazoglou, A.J. and Elnashai, A.S. (1996), "Analytical and field evidence of the damaging effect of vertical earthquake ground motion", *Earthq. Eng. Struct. Dyn.,* **25**(10), 1109-1137. https://doi.org/10.1002/(SICI)1096-9845(199610)25:10<1109::AID-EQE604>3.0.CO;2-0

Riley, M.A., Reinhorn, A.M. and Nagarajaiah, S. (1998), "Implementation issues and testing of a hybrid sliding isolation system", *Eng. Struct.*, **20**(3), 144-154. https://doi.org/10.1016/S0141-0296(97)00079-5

Ramadan, K.S., Sameoto, D. and Evoy, S. (2014), "A review of piezoelectric polymers as functional materials for electromechanical transducers", *Smart Mater. Struct.*, **23**(3), 033001. http://dx.doi.org/10.1088/0964-1726/23/3/033001r

Sankaranarayanan, R. and Medina, R.A. (2007), "Acceleration response modification factors for nonstructural components attached to inelastic moment-resisting frame structures", *Earthq. Eng. Struct. Dyn.*, **36**(14), 2189-2210. https://doi.org/10.1002/eqe.724

Shimada, T., Fujiwaka, T., Moro, S. and Ikutama, S. (2004), "Study on three-dimensional seismic isolation system for next-generation nuclear power plant hydraulic three-dimensional base isolation system", *Proceedings of the 13th World Conference on Earthquake Engineering*, No. 788, Vancouver, BC, Canada, August.

Song, G., Sethi, V. and Li, H.N. (2006), "Vibration control of civil structures using piezo-ceramic smart materials: A review", *Eng. Struct.*, **28**(11), 1513-1524. https://doi.org/10.1016/j.engstruct.2006.02.002

Soni, D.P., Mistry, B.B., Jangid, R.S. and Panchal, V.R. (2011), "Seismic response of the double variable frequency pendulum isolator", *Struct. Control Health Monitor.*, **18**(4), 450-470. https://di.org/10.1002/stc.384

Taniguchi, T. and Miwa, T. (2004), "Slip displacement analysis of freestanding rigid bodies subjected to earthquake motions", *Proceedings of the 13th World Conference on Earthquake Engineering*, Vancouver, BC, Canada, August, Paper No. 437.

Tsuji, Y., Sasaki, T., Waters, T., Fujito, K. and Wang, D. (2014), "A Nonlinear Vibration Isolator Based on a Post-buckled Inverted L-shaped Beam", *Proceedings of the Sixth World Conference on Structural Control and Monitoring*, No. 376, Barcelona, Spain, July.

Wang, T., Li, J. and Wang, F. (2015), "Experimental study on thick rubber bearings of three-dimensional isolation of nuclear power plants", *Nuclear Power Eng.*, **36**(5), 37-40. http://dx.doi.org/10.13832/j.jnpe.2015.05.0037

Xu, Z.D., Tu, Q. and Guo, Y.F. (2011), "Experimental study on vertical performance of multidimensional earthquake isolation and mitigation devices for long-span reticulated structures", *J. Vib. Control*, **18**(13), 1971-1985. https://doi.org/10.1177/1077546311r429338

Yang, J.N., Akbarpour, A. and Ghaemmaghmi, P. (1987), "New optimal control algorithms for structural control", *J. Eng. Mech.*, **113**(9), 1369-1386. https://doi.org/10.1061/(ASCE)0733-9399(1987)113:9(1369)

Zhou, Z., Wong, J. and Mahin, S. (2016), "Potentiality of using vertical and three-dimensional isolation systems in nuclear structures", *Nuclear Eng. Technol.*, **48**(5), 1237-251. https://doi.org/10.1016/j.net.2016.03.005

BS